The Plant Cell, Vol. 18, 852–866, April 2006, www.plantcell.org © 2006 American Society of Plant Biologists

The *TORNADO1* and *TORNADO2* Genes Function in Several Patterning Processes during Early Leaf Development in *Arabidopsis thaliana* [W]

Gerda Cnops,[a] Pia Neyt,[a] Jeroen Raes,[a] Marica Petrarulo,[a] Hilde Nelissen,[a] Nenad Malenica,[b] Christian Luschnig,[b] Olaf Tietz,[c] Franck Ditengou,[c] Klaus Palme,[c] Abdelkrim Azmi,[d] Els Prinsen,[d] and Mieke Van Lijsebettens[a,1]

[a] Department of Plant Systems Biology, Flanders Interuniversity Institute for Biotechnology, Ghent University, B-9052 Gent, Belgium

[b] Institute for Applied Genetics and Cell Biology, Universität für Bodenkultur-Wien, A-1190 Vienna, Austria

[c] Institut für Biologie II und Zentrum für Angewandte Biowissenschaften, Universität Freiburg, D-79104 Freiburg, Germany

[d] Laboratory for Plant Biochemistry and Physiology, Department of Biology, University of Antwerp, B-2020 Antwerpen, Belgium

In multicellular organisms, patterning is a process that generates axes in the primary body plan, creates domains upon organ formation, and finally leads to differentiation into tissues and cell types. We identified the *Arabidopsis thaliana TORNADO1* (*TRN1*) and *TRN2* genes and their role in leaf patterning processes such as lamina venation, symmetry, and lateral growth. In *trn* mutants, the leaf venation network had a severely reduced complexity: incomplete loops, no tertiary or quaternary veins, and vascular islands. The leaf laminas were asymmetric and narrow because of a severely reduced cell number. We postulate that the imbalance between cell proliferation and cell differentiation and the altered auxin distribution in both *trn* mutants cause asymmetric leaf growth and aberrant venation patterning. *TRN1* and *TRN2* were epistatic to *ASYMMETRIC LEAVES1* with respect to leaf asymmetry, consistent with their expression in the shoot apical meristem and leaf primordia. *TRN1* codes for a large plant-specific protein with conserved domains also found in a variety of signaling proteins, whereas *TRN2* encodes a transmembrane protein of the tetraspanin family whose phylogenetic tree is presented. Double mutant analysis showed that TRN1 and TRN2 act in the same pathway.

INTRODUCTION

Leaves originate as lateral outgrowths at the peripheral zone of the shoot apical meristem (SAM). The *SHOOT MERISTEMLESS* (*STM*) gene is important for the maintenance of stem cells of the central zone of the SAM in an indeterminate state. *ASYMMETRIC LEAVES1* (*AS1*) represses *STM* in stem daughter cells at the peripheral zone of the SAM, gradually specifying this region for organogenesis. AS1 is a Myb transcription factor important for many processes during leaf formation: initiation, lateral growth, lamina symmetry, venation patterning, and dorsoventrality (Byrne et al., 2000; Semiarti et al., 2001; Iwakawa et al., 2002, Zgurski et al., 2005). Mutations in *AS1* of *Arabidopsis thaliana* result in asymmetric leaves (Byrne et al., 2000).

In *Arabidopsis*, leaf venation patterning is an early, progressive, and hierarchical process (Candela et al., 1999) in which vascular cells have faster cell cycling than other cell types to get the vascular pattern correctly integrated into the context of nonvascular tissue. The duration of cell cycling, as observed with the *PCYCB1-1*:β-glucuronidase (*GUS*) marker gene, also reflects the size of the different vein types (Kang and Dengler, 2002). Auxin distribution and transport play an important role in venation patterning. In early developmental stages, cotyledon-derived indole-3-acetic acid (IAA) has been suggested to be imported acropetally into the SAM and the first leaf primordia, resulting in the formation of the midvein. Upon maturation, primordia are transformed into IAA sources, which coincide with IAA biosynthesis, first at the leaf tip and then followed by auxin production at the margins (hydathodes). This sink–source transition coincides with the lateral growth of primordia and the formation of the secondary veins, starting apically from the midvein (Avsian-Kretchmer et al., 2002). At a later stage, free auxin is also produced at low levels in the leaf lamina, inducing the tertiary and quaternary veins (Aloni et al., 2003). The key role of auxin in venation patterning has further been proven by pharmacological tests and mutational analysis (for review, see Turner and Sieburth, 2002).

In plants, patterning is a position-dependent process that involves cell-to-cell communication and the establishment of gradients, such as those of auxins, that are recognized and interpreted by cells. These recognition events involve the activation of receptor molecules, resulting in a signal transduction cascade

[1] To whom correspondence should be addressed. E-mail mieke.vanlijsebettens@psb.ugent.be; fax 32-9-33-13-809.
The author responsible for distribution of materials integral to the findings presented in this article in accordance with the policy described in the Instructions for Authors (www.plantcell.org) is: Mieke Van Lijsebettens (mieke.vanlijsebettens@psb.ugent.be).

[W] Online version contains Web-only data.

Article, publication date, and citation information can be found at www.plantcell.org/cgi/doi/10.1105/tpc.105.040568.

and the activation/repression of a number of genes. Well-known examples of receptor molecules are the membrane-localized receptor kinases (Diévart and Clark, 2004) and the cytoplasmic or membrane nucleotide binding site–leucine-rich repeat (NBS-LRR) proteins, of which a number are involved in pathogen recognition (Belkhadir et al., 2004). Tetraspanins represent another type of membrane protein that participates in diverse communication processes, such as cell proliferation, differentiation, and virus and toxin recognition (Hemler, 2003). Recently, a plant tetraspanin has been described with a function in development (Olmos et al., 2003).

Previously, we identified the *tornado* (*trn*) class of recessive mutations that interfere with overall plant growth and morphogenesis (Cnops et al., 1996). Allelism tests showed that there are two genetic loci, *TRN1* and *TRN2*, both located on the lower arm of chromosome 5 (Cnops et al., 2000) and that *trn1* is allelic to *lopped1* (Carland and McHale, 1996; Cnops et al., 2000). A table of the two loci with their different alleles has been presented by Cnops et al. (2000). *TRN* genes are required for root hair patterning and for the suppression of lateral root cap identity in the epidermis (Cnops et al., 2000). Here, we report the isolation of the *TRN1* and *TRN2* genes and their functional analysis in leaf development.

RESULTS

TRN1 Is a Putative LRR Protein and *TRN2* Encodes a Transmembrane Protein

The *TRN1* gene was cloned from a T-DNA–tagged mutant (*trn1-4*) with a T-DNA insertion in At5g55540 (Figure 1A). It encodes a unique *Arabidopsis* gene consisting of two large exons separated by a small intron of 79 bp. TRN1 is classified as an unknown protein of 1380 amino acids. The N-terminal region contains a putative LRR ribonuclease inhibitor–like (LRR-RI) subfamily domain that is most similar to the animal cytosolic nucleotide binding oligomerization domain (NOD-LRR) proteins (Inohara et al., 2005). The LRR domain is followed by an ATP/GTP binding motif A (=P loop) (Figure 1A), which is part of a region homologous with the animal DEATH-ASSOCIATED PROTEIN KINASE1 (DAPK1), as predicted by Structural Classification of Proteins and BLAST. However, the kinase domain, the ankyrin domains, and the death box from DAPK1 were absent in TRN1 (Figure 1A). Most topology prediction programs (including the transmembrane hidden Markov model [TMHMM]) predict TRN1 to be cytosolic. The presence of ESTs and/or genomic sequences in monocots, dicots, and pine (*Pinus taeda*) indicated that TRN1 is conserved in plants and already existed before the evolutionary angiosperm–gymnosperm split. Sequence analysis of *trn1-1* and *trn1-2*/*lop1* revealed deletions of 41 and 23 bp, respectively, followed by a stop codon. Similarly, the C-to-T substitution in *trn1-3* introduced a stop codon into the TRN1-coding region (Figure 1A). Thus, all mutant *TRN1* alleles analyzed to date might arise as a result of a premature translational termination (Figure 1A). Although the position of the stop codon varied from amino acid 96 in *trn1-3* to amino acid 1162 in *trn1-1*, similar phenotypes were observed in all alleles.

The *TRN2* gene was cloned with a map-based strategy (Peters et al., 2004) (see Supplemental Figure 1 online) and corresponded to At5g46700 that had been identified previously by Olmos et al. (2003). The TRN2 protein consists of 269 amino acids and was predicted to be a secreted protein (TargetP score of 0.922) containing four transmembrane domains (TM1 to TM4), two extracellular loops (ECL1 and ECL2), and cytoplasmic N and C termini (Figure 1B; see Supplemental Figure 2 online). Protein alignments identified TRN2 as a member of the tetraspanin family (PF0035). *TRN2* was sequenced in six *trn2* alleles. The single-base changes in the coding region of *trn2-1*, *trn2-2*, and *trn2-3* were situated in the very conserved region of the putative second ECL2 domain (Figure 1B). The G-to-A change in *trn2-1* introduced a stop codon at the beginning of exon 2, leading to a truncated protein that lacked part of the ECL2 loop, the last transmembrane domain, and the cytoplasmic tail (Figure 1B; see Supplemental Figure 2 online). The G-to-A substitution in *trn2-2* replaced a Gly by a Glu. This Gly is conserved in 10 of 17 TRN2-like proteins and followed a very conserved Cys (see Supplemental Figure 2 online). The C-to-T change in *trn2-3* substituted a Pro (conserved in 9 of 17 TRN2-like proteins) for a Leu (see Supplemental Figure 2 online). The 30-bp deletion in *trn2-4* completely removed the small helix in the cytoplasmic tail (Figure 1B). The *trn2-5* allele contained rearrangements, because we were unable to amplify the complete gene by PCR. *trn2-6* had a 4-bp insertion in the ECL2 loop, causing a frameshift and a premature stop codon five amino acids after the insertion. All *trn2* alleles had similar overall phenotypes, indicating that both the ECL2 domain and the C-terminal cytoplasmic tail are important for a functional TRN2 protein.

RT-PCR expression analysis revealed that both *TRN1* and *TRN2* were expressed in seedlings, roots, leaves, stems, flowers, and cell suspensions (Figure 1C). This observation was in agreement with the pleiotropic phenotype of both *trn* mutants. RNA in situ hybridizations were performed on 11-d-old seedlings. Strong expression of *TRN1* and *TRN2* was detected in the SAM and the young leaf primordia (Figure 1D). Expression was also detected in the lamina of the cotyledons, especially in the mesophyll and vascular bundles (Figure 1D).

The Plant Tetraspanin Family Consists of Several Members and Is Conserved throughout the Multicellular Clades

BLAST and HMMER (profile of hidden Markov models for protein sequence analysis) searches revealed 16 homologs of *TRN2* in *Arabidopsis* (see Supplemental Figure 2 online) and plenty of homologs in a variety of plant species, including mosses (*Physcomitrella* and *Ambronella*), gymnosperms (*Cycad* and *Pinus* species), and angiosperms (both monocots and dicots). Therefore, we refer to TRN2 also as *Arabidopsis* TETRASPANIN1 (TET1). All plant tetraspanins have a similar predicted structure: four transmembrane domains with a short ECL1 of ~11 amino acids between TM1 and TM2, a large ECL2 of ~137 amino acids between TM3 and TM4, and short and divergent N- and C-terminal tails with 6 to 8 and 7 to 40 amino acids, respectively (as can be deduced from the non-full-length plant ESTs) (Figure 1B; see Supplemental Figure 2 online). Protein sequences derived from 40 clustered EST/cDNAs were used together with predictions from the annotated rice (*Oryza sativa*) pseudomolecules

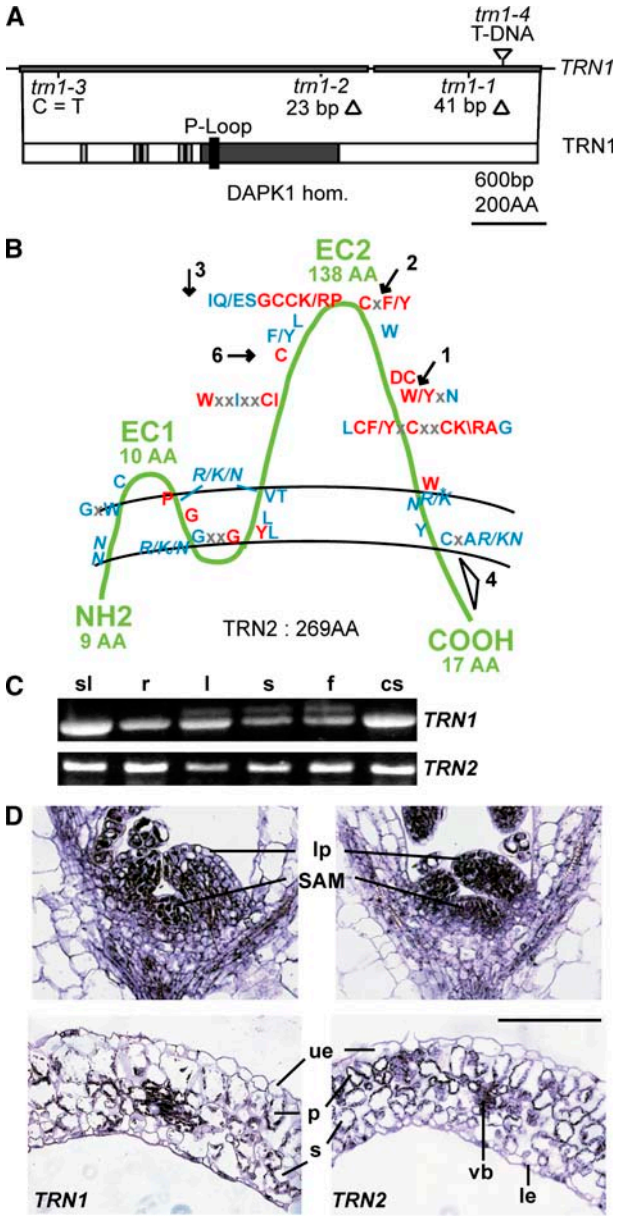

Figure 1. *TRN1* Gene Structure and *TRN* Gene Expression.

(A) Genomic and protein structures of *TRN1*. Top line, gene structure of *TRN1* with two boxed exons and a small intron. The positions of the mutations in each of the four *trn1* alleles are represented. Bottom line, TRN1 protein with LRR–ribonuclease inhibitor-like repeat domains (gray boxes), a P-loop for ATP/GTP binding (black box), and homology with DAPK (dark gray box). AA, amino acids.

(B) Structure of the TRN2/TET1 protein as a representative of the plant TET family based on comparisons of 10 *Arabidopsis* TET proteins and 51 TET proteins derived from full-length tomato (*Lycopersicon esculentum*), soybean (*Glycine max*), daylily (*Hemerocallis hybrid*), ice plant (*Mesembryanthemum crystallinum*), maize (*Zea mays*), wheat (*Triticum aestivum*), barley (*Hordeum vulgare*), and rice (*Oryza sativa*) cDNA and rice genomic sequences (all members of the five conserved plant tetraspanin classes). The most conserved amino acids are positioned along the protein. Residues that are 100% identical among different plants are in red, and those that are 90% identical are in blue. The polar amino acids in the four transmembrane domains are in italics.

(C) Expression analysis of *TRN1* and *TRN2*. RT-PCR analysis of *TRN2*/*TET1* with exon 1 and 2 primers. cs, cell suspensions; f, flowers; l, leaves; r, roots; s, stems; sl, seedlings.

(D) In situ localization of *TRN1* and *TRN2* in 7-d-old seedlings. Top two panels are SAMs hybridized with antisense *TRN1* (left) and *TRN2* (right) probes; bottom two panels are sections through the cotyledon lamina hybridized with the same probes. le, lower epidermis; lp, leaf primordia; p, palisade parenchyma; s, spongy parenchyma; SAM, shoot apical meristem; ue, upper epidermis; vb, vascular bundle. Bar = 200 μm.

(version 1; available at http://www.tigr.org/) and the 17 *Arabidopsis* genes to make an evolutionary tree of the complete plant TET protein family (Figure 2; see Supplemental Figure 3 online). Ten of the 17 *Arabidopsis* TET proteins could be grouped reliably into five classes amid TETs of both monocot and eudicot species (Figure 2). All of these proteins contained the absolutely (100%) and highly (90%) conserved amino acids, such as the Cys in ECL1, three amino acids before TM2, and the nine Cys residues in ECL2, indicating that these residues were important for functionality (Figure 1B). All 10 *Arabidopsis* genes from these five classes were expressed (Figure 2). The remaining seven *Arabidopsis* TET proteins were more divergent and were less obvious to classify. Their position in the tree varied depending on the methodology used, and no clear homologs could be found in other plant species (Figure 2). Some of these proteins had an accelerated evolutionary rate (Figure 2), resulting even in mutations that affected domain length or residues that were completely conserved in the other plant TET proteins. Few expression data (EST or microarray) were available for this group of genes, and no homologs were found in the rice genome, suggesting that they could be dicot-specific. Genevestigator (https://www.genevestigator.ethz.ch) gave expression only above background for *Arabidopsis* TET11, TET12, and TET13 in cell suspensions, roots, and stamens, respectively, which might be the reason for the lack of ESTs in other dicot species. Because no expression data were obtained for *Arabidopsis* TET16 and TET17, they might represent pseudogenes.

Comparison of secondary structure between the plant TET proteins and the tetraspanins revealed that both groups of proteins were of similar size and shared the same topology. These results indicate that the plant TET family shares structural homology with the tetraspanin family in animals.

trn Leaves Are Defective in Symmetry and Size

All *trn* mutants, irrespective of their genetic background and mutated either in the *TRN1* or the *TRN2* locus, had similar overall phenotypes: severely dwarfed, with twisted and malformed organs, and sterile. However, cotyledon shape and symmetry were unchanged. Total length, lamina length, and lamina area were normal in *trn2-1*, and only the lamina area was slightly, but significantly, reduced in *trn1-1* (6.1 mm^2 compared with 6.8 mm^2 in C24). Rosette leaf size and shape were severely affected. *trn* leaves had a rumpled surface with asymmetric laminas because of nondeveloped blade parts. These defects varied within and

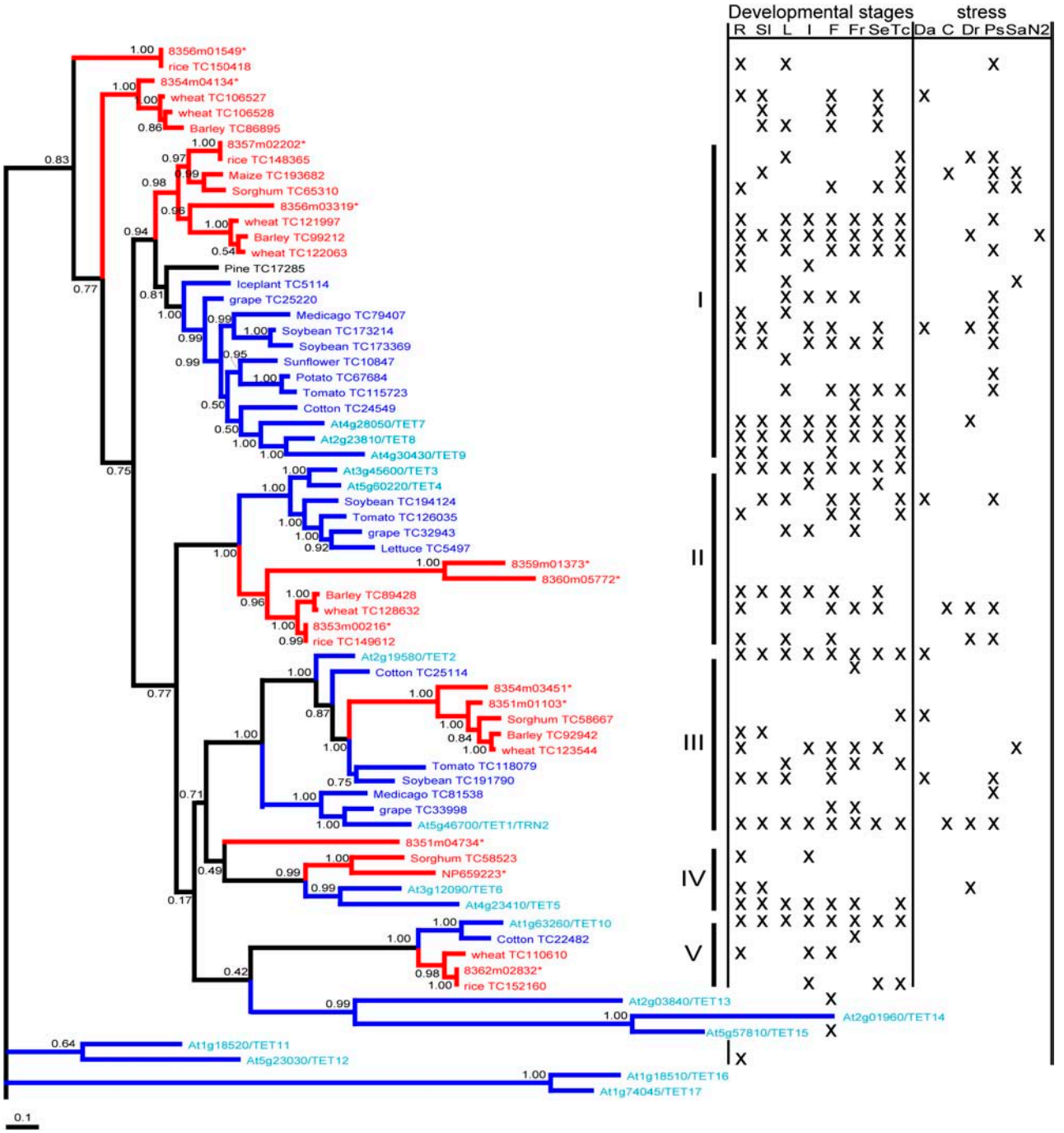

Figure 2. Phylogenetic Tree of the Plant Tetraspanin Family, Inferred with MrBayes.

Posterior probability values are shown at the internodes. The scale measures the evolutionary distance in substitutions per amino acid site. The neighbor-joining analysis yielded similar classes, although deeper nodes were less supported. In addition, the branch containing *Arabidopsis* TET13 to TET15 branched off at the base of the tree. Because of this incongruence between the two methods, and the low posterior probability values in the Bayesian analysis, the positions of these genes remained uncertain; therefore, they were not assigned to any of the defined classes. The tree was based on 40 plant-deduced protein sequences obtained from the TIGR gene indices database, the 17 *Arabidopsis* TET proteins, and predictions from rice genomic clones (asterisks). Genes from monocots are indicated in red, from dicots in dark blue, and from *Arabidopsis* in light blue. EST data are given next to the genes. The *Arabidopsis* data set was completed with the Gene Atlas data from Genevestigator (https://www.genevestigator.ethz.ch/). C, cold stress; Da, grown in darkness; Dr, drought stress; F, flowers; Fr, fruits; I, inflorescences; L, leaves; N2, nitrogen starvation; Po, pool of conditions; Ps, pathogen response; R, roots; Sa, salt stress; Se, seed; Sl, seedling; Tc, tissue culture. In the analysis, 22K array data were used.

between individuals (i.e., parts or even the entire leaf blade could be missing) (Figure 3A). The length of the first and second leaves was slightly reduced in *trn1-1* but unaffected in *trn2-1*. However, subsequent rosette leaf laminas were visibly smaller in both *trn* mutants. Lamina area was reduced by two-thirds in the first leaves of *trn1* and *trn2* (Figure 3B) because of a decrease in cell number. The palisade cell number in transverse sections of fully expanded *trn2-1* leaves was 44 ± 5, compared with 120 ± 5 in Columbia 4 (Col). The reduction in cell number in *trn2* was partially compensated by larger cells (Figure 3E). In addition, the upper epidermal cell area was increased in *trn2-1* compared with Col (5264 ± 658 μm^2 versus 2146 ± 258 μm^2). Dorsoventrality was normal, as suggested by the occurrence of a vacuolated abaxial rib zone, a meristematic adaxial side in young leaf primordia, and the presence of palisade and spongy parenchyma and collateral vascular bundles with dorsal xylem and ventral phloem in expanded leaves (Figures 3D and 3E).

Serial transverse sections through the shoot apices of 6-d-old seedlings showed that lateral meristems of the leaf primordia were reduced in *trn2-1* and often contained vacuolated cells, resulting in truncated lateral outgrowths in older primordia with differentiated cells or even intercellular gaps (Figure 3D). At full expansion, big intercellular gaps, depleted in palisade and spongy cells, were present throughout the leaf (Figure 3E).

A flow cytometry experiment was performed with the first two true leaves of the *trn* mutants (*trn1-2* and *trn2-4*) in Wassilewskija (Ws) and heterozygous wild-type plants (Ws1 and Ws2) to assess whether changes in mitotic cell division or endoreduplication could be observed and to explain the altered expansion and differentiation in *trn* mutants (Figure 3F). Whole-leaf samples were harvested from 8 to 25 d after germination (DAG) to analyze the DNA content as a function of time. At early time points, most cells were in mitotic cell division with a 2C or 4C DNA content, representing the cells in the G1- or G2-phase of the cell cycle, respectively. The transition from mitotic cell division to expansion was characterized by the increase of higher ploidy levels and thus coincided with the start of endoreduplication (Beemster et al., 2005). The leaves reached maturity when the DNA content was stabilized. When these different processes were monitored in the *trn* plants, it became evident that the transition from mitotic cell division to endoreduplication occurred at least 2 d earlier in the mutants. The 2C/4C content was stable in wild-type plants until 10 DAG, whereas in *trn* mutants it had already decreased before 8 DAG. The leaves of the *trn* mutant also reached maturity at 15 DAG, whereas in wild-type leaves the stable DNA distribution was seen only at 19 DAG. These data showed that the transition from mitotic cell division to cell expansion occurred earlier in the *trn* mutants (Figure 3F). The basipetal progression in proliferation, expansion, and differentiation in the leaf blade that can be visualized with the cell cycle marker PCYCB1-1:GUS in young primordia shows a gradual restriction of mitotically active cells toward the base of the leaf in the course of organ differentiation (Donnelly et al., 1999). A similar spatial distribution of PCYCB1-1:GUS activity became apparent when analyzing *trn1-1*, although ectopic activity was noted in the vascular system (see below).

trn Cotyledons and Vegetative Leaves Have a Defective Venation Network

Venation patterning was abnormal in the majority of mutant cotyledons. The complexity was measured as the number of secondary vein loops originating from the midvein: 87% of *trn1-1*, 73% of *trn1-2*, 62% of *trn2-1*, and 80% of *trn2-4* cotyledons had the lowest complexity (i.e., two secondary loops plus or minus the start of one or two others), whereas wild-type cotyledons (except C24) had three or four secondary loops (Figure 4). Furthermore, the venation network was discontinuous. The secondary loops were not connected apically to the midvein in ~20% (*trn2-1* and *trn2-4*) to 25% (*trn1-1* and *trn1-2*) of the cotyledons (Figure 4). Interestingly, vascular islands, veins unconnected to the rest of the network, were detected in a small subset of *trn* cotyledons (Figure 4).

The provascular marker line *PATHB8*:*GUS* was used to distinguish between patterning and differentiation defects in *trn2-1* leaves. At 5 DAG, preprocambial (isodiametric) cells were stained in the middle of the leaf primordium at the position of the future midvein in wild-type leaves as well as in *trn2-1* mutants (Figure 5A). Abnormalities appeared at 6 DAG and coincided with the formation of the secondary vein loops. Although in wild-type leaves the secondary veins always formed closed loops, they did not connect apically or distally or, in extreme cases, at all to the midvein in *trn2-1* leaves (Figure 5A). Tertiary and quaternary veins were formed in leaves 1 and 2 of Col within and outside the secondary vein loops at 7 and 8 DAG, respectively. By contrast, in *trn2-1* mutants, almost no higher-order veins were initiated. Similar observations were made using differential interference contrast optics in *trn1-1* and *trn2-1* primordia (data not shown). The PCYCB1-1:GUS activity was strong in *trn1-1* in and around differentiated veins, especially at open vein endings and in vascular islands in differentiated apical zones. Ectopic expression revealed that these cells were still dividing or blocked at the G2/M transition of the cell cycle. This ectopic expression coincided with thicker veins (Figure 5B), suggesting that in these cells division takes longer than in wild-type cells.

Venation complexity in first leaves was measured as the number of branch points (brp) between veins. The total number of brp was 80 and 90% reduced in *trn1-1* and *trn2-1*, respectively, but this was attributable not only to the decreased lamina area in both mutants, because the brp:lamina area ratio was 57% that of wild type in *trn1-1*, 39% in *trn1-2*, 33% in *trn2-1*, and 38% in *trn2-4* (Figure 3C). To identify the type of veins that were affected, we counted the brp between different order veins. There were 60% fewer brp between primary and secondary veins and 75% fewer between secondary and tertiary veins than in the wild type, but almost no tertiary to quaternary brp in either mutant (Figure 3A). Hence, in the *trn* mutants, the total number of brp decreased mainly because of the progressive reduction in higher-order veins. The midvein itself was never affected. It should be noted that the total number of brp, the brp:lamina area ratio (Figure 3C), and the total number of secondary vein loops (open and closed) were similar in both *trn* mutants.

In addition to the complexity of the vascular network, its continuity was also affected in *trn* mutants, because open distal vein loops were detected and vascular islands were observed in

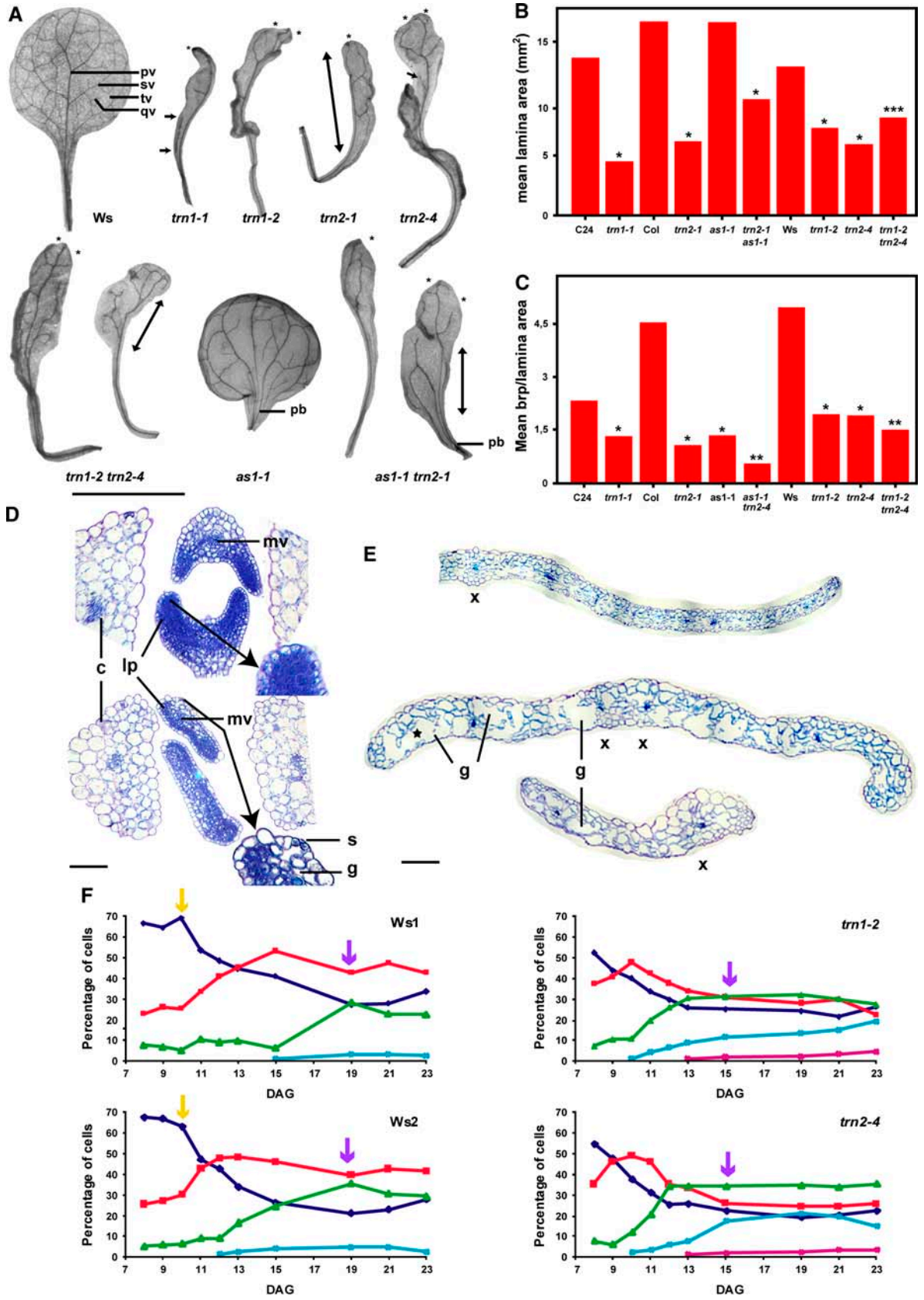

Figure 3. Morphology and Anatomy of *trn* Mutants.

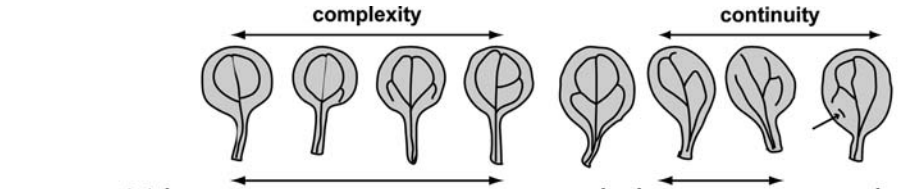

genotype	total no of cots	simpler venation pattern				maximal complexity	open top loop		vascular island
C24	68	20	[25]	[25]	[25]	6	0	0	0
trn1-1	90	[59]	22	6	13	1	(27)	3	(6)
WS	101	2	5	19	30	[45]	0	0	0
trn1-2	170	[34]	29	10	24	3	(23)	0	(4)
trn2-4	85	[39]	32	9	18	2	(21)	0	ND
trn1-2 trn2-4	51	9	[39]	12	[39]	0	(12)	0	ND
Col	67	0	12	25	24	[39]	1	0	0
trn2-1	66	15	[32]	15	23	15	(17)	0	(5)
as1-1	67	[48]	24	7	15	4	(15)	0	0
as1-1 trn2-1	113	[60]	20	3	15	2	(46)	(9)	ND
as1-1 trn1-1	46	[30]	24	11	[35]	0	(24)	(24)	ND

Figure 4. Venation Pattern in Cotyledons of *trn* Mutants.

The venation complexity is given as the percentage of cotyledons displaying a particular venation pattern. The most representative complexity for a wild type or mutant is boxed. The percentages of cotyledons with discontinuities in their venation are circled. The arrow indicates a vascular island. cots, cotyledons; ND, not determined.

>50% of *trn1-1* and *trn2-1* first leaves. These nonconnected pieces of vasculature were completely absent in both C24 and Col wild types. The discontinuous venation network was investigated with aniline blue, a dye that stains callose in phloem sieve elements. The gaps did not contain phloem elements and were thus completely deprived of vascular tissue (Figure 5F). This observation is in agreement with the discontinuity between vascular elements seen in the *PATHB8*:*GUS* marker analysis (Figure 5A).

trn1 and *trn2* Double Mutant Analysis

To investigate the genetic interaction between *trn1* and *trn2*, double mutants were made. Heterozygous plants for both *trn1-2* (Ws) and *trn2-4* (Ws) were crossed because both mutants are sterile. In the next generation, F1 plants heterozygous for both *trn1-2* and *trn2-4* were selected with PCR analysis, and seeds were harvested. Because *TRN1* and *TRN2* are only separated by 3545 kb on the bottom arm of chromosome 5, very few double mutants were expected in the F2 generation. Therefore, 113 wild-type-looking plants were analyzed by PCR, and the 101 plants heterozygous for both *trn1* and *trn2* were harvested. Only one plant segregated in the next generation with the ratio of 1:3 mutant:wild type, indicating that the parental plant had undergone a crossover between *TRN1* and *TRN2*. No obvious phenotype different from those of *trn1-2* or *trn2-4* was observed in the next generation. To analyze the leaf shape and venation phenotypes in more detail, the cotyledons and first two leaves of 39 F3 *trn*-looking plants were harvested. The remaining leaves were collected for DNA preparation, and the genotype of each plant was verified with PCR to be a double mutant. The cotyledons and first leaf pair in *trn1-2 trn2-4* looked indistinguishable from those of the single parents. The leaf surfaces were irregular, with pieces or even half of the lamina missing (Figure 3A). The lamina area of the double mutant was similar to that of *trn1-2* and statistically slightly larger than that of *trn2-4* (Figure 3A). The double mutant had a similar but slightly less severe venation pattern in the cotyledons compared with both single mutants (Figure 4). The vasculature of the double mutant leaves was severely reduced and mostly open. The number of brp was similar to that of both single mutants (data not shown), but the brp:lamina area ratio

Figure 3. (continued).

(A) Leaf morphology and venation pattern of first leaves of Ws, *trn1-1*, *trn1-2*, *trn2-1*, *trn2-4*, *trn1-2 trn2-4*, *as1-1*, and *trn2-1 as1-1*. Double-headed arrow, part of the leaf blade missing = asymmetry; asterisk, open top loop. pb, primary bundle; pv, primary vein or midvein; qv, quaternary vein; sv, secondary vein; tv, tertiary vein. Bar = 0.5 cm.

(B) and **(C)** Graphs of the lamina area **(B)** and total branch points (brp)/lamina area **(C)** of fully expanded first and second leaves of 30 C24, 58 *trn1-1*, 30 Col-4, 41 *trn2-1*, 39 *as1-1*, 37 *trn2-1 as1-1*, 23 Ws, 31 *trn1-2*, 34 *trn2-4*, and 50 *trn1-2 trn2-4* plants. Single, double, and triple asterisks indicate significant differences between mutant and parent by Student's *t*-test ($P < 0.05$) and between double mutants and both parental single mutants.

(D) Transverse sections through 8-d-old shoot apices of wild-type (top) and *trn2-1* (bottom) leaf primordia, respectively. c, cotyledon; g, gap; lp, leaf primordium; mv, midvein; s, stomata. Bar = 300 μm.

(E) Transverse sections through fully expanded first leaves of wild-type (top) and two *trn2-1* (bottom) laminas. x indicates the position of the midvein, which is bifurcated in the top leaf and eccentric in the bottom *trn* leaf. Bar = 200 μm.

(F) Whole-leaf flow cytometry of the wild type (Ws) and *trn* mutants. The different stages of leaf growth are indicated with arrows: proliferation period before the yellow arrow, expansion period between the two arrows, and mature stage after the purple arrow. DAG, days after germination.

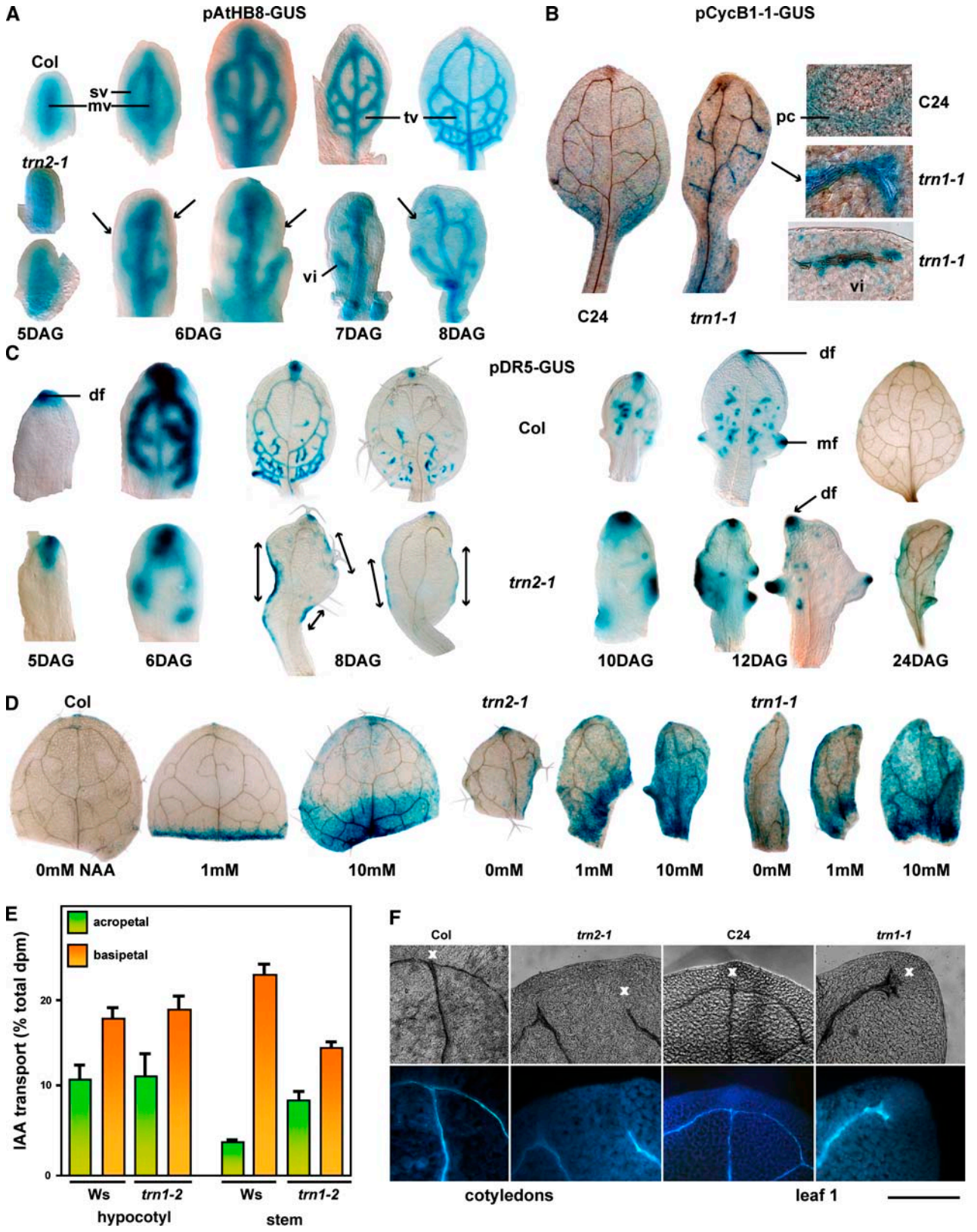

Figure 5. Venation Patterning in Leaves of *trn* Mutants.

was statistically more reduced in *trn1-2 trn2-4* compared with the single mutants (Figure 3A). These data indicate that TRN1 and TRN2 are involved in the same processes. Because of the similar phenotypes of the single mutants, epistasy could not be determined.

TRN1 and *TRN2* Are Epistatic to *AS1* with Respect to Leaf Asymmetry, and *TRN2* Is Synergistic with *AS1* with Respect to Venation Patterning

The *as1-1* mutant develops leaf laminas with unequal left and right halves, petioles attached to the abaxial surface of the leaf blades, and altered venation patterning (Figure 3A) (Byrne et al., 2000; Sun et al., 2002; Zgurski et al., 2005). *trn2-1* (Col) was crossed to *as1-1* (Col-1), and plants homozygous for *as1-1* were self-fertilized in the F2 and analyzed in the F3 for the phenotype of *trn2-1 as1-1*. In a similar manner, double mutants were obtained from a cross between *trn1-1* (C24) and *as1-1*. Similarly, *trn2-1 as1-1* and *trn1-1 as1-1* segregated 1:3 and had a clear *trn* leaf shape phenotype, with the typical missing parts in the lamina and no characteristics of *as1-1* leaf shape (Figure 3A). These data reveal that *TRN2* and *TRN1* are epistatic to *AS1* with respect to leaf asymmetry. However, total leaf length and lamina area in *as1-1 trn2-1* were intermediate compared with those of their parents, indicating that with respect to lamina growth both loci were independent (Figure 3B).

The vascular system was analyzed in the cotyledons to exclude the influence of the aberrant leaf shape on venation pattern. The reduction in venation complexity produced in *as1-1* and *trn2-1* single mutants was even more pronounced in the double mutant (Figure 4). Furthermore, twice as many double mutant cotyledons had an open apical loop, and a new phenotype of two open apical loops was observed in 9% of *as1-1 trn2-1* cotyledons (Figure 4). A similar trend was seen in the first leaves as well, where the brp:lamina area ratio was more reduced in the double mutant than in both single mutants (Figure 3C). These data indicate that the *TRN2* and *AS1* loci act synergistically in venation patterning. The analysis of the vasculature in *trn1-1 as1-1* was more complicated, probably because of the mixed background of both single mutations. *TRN1* and *AS1* probably also act synergistically in venation patterning, because the new phenotype of two open apical loops was observed in 24% of the *trn1-1 as1-1* plants.

trn Mutants Have an Altered Auxin Distribution

Auxin is an important inducer of vascular pattern formation, and this pattern is severely affected in *trn* mutants. Therefore, the altered venation patterning in *trn* leaves could result from defects in auxin homeostasis, distribution, or transport. The *PDR5*:*GUS* marker gene was introgressed into *trn1-1* and *trn2-1* for in situ localization of auxin accumulation or auxin reactivity in leaves (Mattsson et al., 2003; Koizumi et al., 2005). In wild-type leaf primordia, *GUS* expression was first noticed in a distal focus and subsequently seen at the position of the future midvein (Figure 5C). With the initiation of the leaf lamina and the differentiation of the midvein, *PDR5*:*GUS* expression diminished from the midvein, and new expression zones appeared at the sites of future secondary vein loops, followed by new zones of expression that coincided with the formation of the tertiary and quaternary veins (Figure 5C) (Mattsson et al., 2003). In wild-type adult leaves, weak *PDR5*:*GUS* expression was observed at the hydathode regions. In addition, a similar pattern was observed in leaves 3 and 4. *PDR5*:*GUS* activity preceded procambium formation, decreased when procambial strands were formed, and disappeared at later stages of vascular differentiation. Until 5 DAG, the *PDR5*:*GUS* expression pattern did not differ between the wild-type and either *trn* mutant, except for the often asymmetric location of the distal focus (Figure 5C). Weaker *PDR5*:*GUS* patterns were obtained in *trn* leaves at 6 DAG, in agreement with the ectopic *PAtHB8*:*GUS* expression pattern at that time. Interestingly, little PDR5:GUS activity was detected at or around the vascular system of 8-d-old leaves 1 and 2, but ectopic expression was observed along the margins and persisted in mature leaves (Figure 5C). Besides the GUS pattern described above, PDR5:GUS activity in later leaves was stronger and 2 d earlier in the marginal serrations than in the wild type (Figure 5C). Serial sections of these leaves showed ectopic GUS activity predominantly in the palisade and spongy mesophyll layers (see Supplemental Figure 4 online). Auxin concentration was measured in shoot apices of 19-d-old seedlings. The endogenous IAA concentration in both *trn* mutants was similar to that of the wild type (65 $\pm$ 15 pmol/g in *trn1-1*, 71 $\pm$ 15 pmol/g in Ws, 26 $\pm$ 11 pmol/g in *trn2-1*, and 41 $\pm$ 9 pmol/g in Col), indicating that there was no reduction in overall auxin concentration in *trn* shoots. To assess the role of the *TRN* genes in auxin response, wild-type and *trn* leaves were treated with α-naphthaleneacetic acid and the

Figure 5. (continued).

(A) 5-Bromo-4-chloro-3-indolyl-β-D-glucuronide (X-Gluc) staining of the *PATHB8*:*GUS* marker gene activity in 5-, 6-, 7-, and 8-d-old first leaves of wild-type and *trn2-1* plants. mv, midvein; sv, secondary veins; tv, tertiary veins; vi, vascular island.

(B) Activity of PCYCB1-1:GUS in *trn1-1*. pc, procambium.

(C) PDR5:GUS activity in 5- to 8- and 24-d-old first leaves (left) and 10- to 12-d-old third leaves (right) of wild-type (top) and *trn2-1* (bottom) plants. df, distal focus; mf, marginal focus. Double-headed arrows indicate ectopic expression.

(D) PDR5:GUS activity in excised 10-d-old Col, *trn2-1*, and *trn1-2* leaves after exposure to 0, 1, and 10 mM α-naphthaleneacetic acid (NAA).

(E) Auxin transport measurements of Ws and *trn1-2/lop1* hypocotyls and stem fragments. The hypocotyls or stem fragments were placed either upside-up (acropetal transport) or upside-down (basipetal = active transport) in [^{3}H]IAA. The pieces were cut in two, and the radioactivity present in the top half was expressed as a percentage of the total amount of radioactive IAA present in the entire explant. For the upside-up direction, 14 (44) WS and 10 (27) *trn1-2/lop1* hypocotyls (stems) were used; for the upside-down direction, 36 (28) Ws and 41 (80) *trn1-2/lop1* hypocotyls (stems) were used. Error bars indicate SE.

(F) Top, differential interference contrast images of xylem patterning of primary and secondary veins at the top of the cotyledon or first leaf of 3-week-old seedlings. Bottom, fluorescence microscopy of phloem sieve tubes stained with aniline blue. x indicates the top of the midvein. Bar = 1 mm.

expression of *PDR5*:*GUS* was examined. Ectopic PDR5:GUS activity was seen at the margins and the wounding site. A similar, but more intense, response was observed in *trn* leaves (Figure 5D).

The defective venation patterning, ectopic PDR5:GUS activity, and altered auxin transport measured in *trn1-2*/*lop1* stem fragments (Carland and McHale, 1996) suggested that auxin transport could also be defective in mutant seedlings. Therefore, the capacity to actively transport auxin was analyzed in hypocotyls of 19-d-old seedlings. Auxin transport in etiolated hypocotyls of *trn1-2*/*lop1* and Ws is summarized in Figure 5E. The amount of actively transported IAA, expressed as the percentage of basipetal minus acropetal transport, was 7.9% in Ws and in *trn1-2*/*lop1* as well. Also, no differences were observed in polar auxin transport rates between *trn1-1* and C24, and no reduced auxin transport was measured in *trn2-4* compared with Ws hypocotyls. However, a threefold reduction in auxin transport was measured in *trn1-2*/*lop1* excised stem fragments compared with Ws fragments. Moreover, we observed a 2.2-fold increase in acropetal transport (Figure 5E).

DISCUSSION

trn1 and *trn2* have similar phenotypes, and double mutant analysis has shown that they are required for related, overlapping signaling events. TRN1 contains domains specific for signaling proteins, and TRN2 is a tetraspanin, a class of proteins known to be involved in cell-to-cell communication in animals. Furthermore, both proteins are produced only in multicellular organisms. Therefore, we argue that both TRN1 and TRN2 act in the same developmental communication pathway.

TRN2/TET1 Is a Member of a Plant-Specific Branch of the Tetraspanins

We isolated the *TRN2*/*TET1* gene and showed that it is a putative transmembrane protein belonging to the family of tetraspanins. These proteins are widely distributed throughout the animal and plant kingdoms, with several homologs in almost all species, although plant tetraspanins are mutually more conserved than their animal counterparts. They all share a very conserved topology that is important for facilitating the interactions between different proteins in animals by stabilizing and rendering large protein complexes functional. Tetraspanins interact with a variety of proteins, such as other tetraspanins, integrins, proteoglycans, growth factors, growth factor receptors, and signaling enzymes (Maecker et al., 1997; Hemler, 2001, 2003). Specifically, the ECL2 domain found in animal tetraspanins seems to be relevant for complex formation with other proteins, as follows from genetic evidence and chimeric protein analysis (Hemler, 2001, 2003; Stipp et al., 2003). Sequence analysis of the different *trn2* alleles revealed the importance of the main ECL2 and the C-terminal end in plant tetraspanins, exactly the same domains considered to be crucial for tetraspanin function in animals. In contrast with animals, plant tetraspanins share nine rather than four, six, or eight completely conserved Cys residues. In plants, these Cys residues could also be involved in the formation of disulfide bridges, as supported by the missense mutations in the *trn2-2* and *trn2-3* alleles. An uncharged amino acid (Pro-164 in *trn2-2* and Gly-177 in *trn2-3*), closely linked to a highly conserved region containing three Cys residues, is exchanged for the charged amino acid Glu. Pro and Gly are important amino acids for secondary structure determination; therefore, mutating these amino acids could interfere with the correct folding of the protein (Cys–Cys interactions). Alternatively, an active site for binding to other protein(s) could be disturbed upon mutation of Pro-164 and Gly-177.

The C-terminal tail of both animal and plant tetraspanins is mostly short (4 to 40 amino acids) and divergent. Nevertheless, mutational and chimeric studies in animals imply an important role for this domain, such as targeting to intracellular locations or interaction with cytoskeletal or signaling molecules, including protein kinase C, integrins, and mu3A subunit AP-3 (Stipp et al., 2003). Our data also assign an important function to this very short domain in plants, because the phenotype of *trn2-4*, in which 10 of 14 amino acids from the C-terminal tail were deleted, is as dramatic as that of the other *trn2* alleles.

Animal tetraspanins contain a number of highly polar residues in TM1, TM2, and TM4 that could be involved in stabilizing the transmembrane tertiary structure for dimerization or multimerization to create the tetraspanin web (Stipp et al., 2003). Seven polar residues are present in TM1 to TM4 of plant tetraspanins (Figure 1B); three other residues are shared between the 50 and 75% of the sequences tested, which could indicate that plant tetraspanins also interact with several tetraspanins in a tetraspanin web.

The phylogenetic tree shows that the divergence of plant tetraspanin classes predates the monocot–dicot split and probably happened before the gymnosperm–angiosperm split (Figure 2). Members of the five distinct classes can be found in mosses, gymnosperms, and angiosperms and are active in different tissues and under abiotic stress conditions. Because all of the absolutely conserved amino acids in plant tetraspanins (Figure 1B) are conserved in the *Physcomitrella* ESTs as well (http://www.moss.leeds.ac.uk/blast.html), they likely have been conserved for >700 million years in all Embryophyta and might be functionally important. Despite some differences between animal and plant tetraspanins, the highly conserved protein topology, protein lengths, and functionality of the ECL2, and the C-terminal tail make the animal and plant tetraspanins very probably derived from a common ancestor. Tetraspanins are membrane-localized in animals (in tetraspanin-enriched microdomains) and participate in diverse communication processes (Maecker et al., 1997; Hemler, 2001, 2003). Therefore, it is not surprising that until now tetraspanins have been restricted to multicellular organisms and unicellular amoebas that can form multicellular structures (Huang et al., 2005) and that homologs are lacking for the unicellular green algae *Chlamydomonas* and yeast. The patterning and growth defects caused by the mutations in TRN2/TET1 suggest that in plants as well as animals, tetraspanins are involved in cell–cell interactions and signaling.

TRN1 Is a Putative LRR Protein

TRN1 encodes an unknown protein with high similarity to NOD-LRR proteins and is predicted to be cytoplasmic. TRN1 is also

homologous with DAPK. However, the kinase domain is not present. Other LRR proteins without kinase domains, such as CLAVATA2 and TOO MANY MOUTHS, have been shown to be required for cellular communication processes that decide between stem cell fate and differentiation fate (Nadeau and Sack, 2003). The NOD-LRR proteins are involved in pathogen resistance in mammals, and a number of these proteins are cytoplasmic and resemble the *R* genes in plant pathogen resistance. NOD-LRR and *R* genes are specificity determinants of the immune response. They act as regulatory modules for protein activation because of the presence of a NBS and serve as protein interaction platforms affected by the LRR domain. The subsequent signaling cascade leads to gene activation (Belkhadir et al., 2004). In TRN1, the putative LRR domain is N-terminally followed by the NBS, which is opposite to the arrangement of these domains in NOD-LRR and R proteins. In any case, the presence of these two domains suggests a role for TRN1 in signaling.

TRN Genes Function in Leaf Symmetry through Auxin Homeostasis

Both *trn1* and *trn2* mutants display similar leaf phenotypes that are related to patterning processes early during leaf development (i.e., lateral symmetry, venation patterning, and lamina outgrowth). *TRN2* and *TRN1* were epistatic to *AS1* with respect to leaf asymmetry, indicating that *TRN2* and *TRN1* act upstream of *AS1* either in the SAM at the leaf initiation site or slightly later in the leaf primordium. Both *TRN* genes are expressed in the SAM and the leaf primordia, as shown by in situ hybridization. Displacement and asymmetry of auxin foci, and hence auxin response patterns, have been proposed to lead to asymmetric vein patterns and asymmetric leaf shape in *as1* and *as2* (Zgurski et al., 2005). Altered *PDR5*:*GUS* expression in *trn* mutants was not only reflected in a shifted positioning of the distal and marginal foci, as in *as1*; in addition, *trn* mutants also exhibited an ectopic and asymmetric distribution of auxin along the leaf margins of expanding leaves (Figure 5C). Auxin homeostasis is important for the correct balance between cell proliferation and expansion, because the sites of highest IAA production coincide with cell division activity. Moreover, a tight control of auxin homeostasis appears to be critical for normal leaf growth as well (Ljung et al., 2001). Thus, the altered auxin distribution in *trn* mutants could severely affect cell division and expansion. Indeed, flow cytometry of leaves and histological sections confirmed such changes in cell division/expansion activity at the stage at which ectopic *PDR5*:*GUS* expression was detected. Changing the balance between cell division, cell expansion, and cell differentiation through local induction of either cell cycle genes or expansins in young leaf primordia resulted in asymmetric leaves with indentations, because of fewer and larger cells and less differentiation of the vasculature (Wyrzykowska et al., 2002; Verkest et al., 2005), or leaf outgrowths (Pien et al., 2001). The similar phenotypes observed in *trn* suggest that the *TRN* genes are essential for the establishment of development, thereby controlling the interplay between cell cycle progression and differentiation. Both *TRN* genes are seemingly required for leaf proliferation and differentiation in a spatiotemporal context.

TRN Genes Are Crucial in Signaling and Sensing the Developmental Stage of Cells

The impaired vasculature is not the consequence of altered leaf morphology because the latter only partially accounts for the reduced vascular complexity and can explain neither the discontinuity nor the incorrect initiation of secondary veins. Furthermore, lamina shape is unaltered in cotyledons, despite the reduced complexity and discontinuity of the vascular system. Both *TRN* genes were synergistic with *AS1* concerning venation patterning, indicating that *AS1* and the *TRN* genes play a role in the process of lateral symmetry as well as in venation patterning, but through different pathways. TRN2 acts early because it is the limiting factor for *PATHB8*:*GUS* expression and procambium formation. Among the different hormones involved in vascular development, auxin plays a key role in vascular pattern formation and acts upstream of the regulator of the early procambium development marker *PATHB8*:*GUS* (Baima et al., 1995). The changed auxin balance in *trn* mutants is not attributable to an overall alteration in auxin concentration but rather results from local changes in auxin reactivity or distribution. *trn* mutants show an enhanced PDR5:GUS activity after the external addition of auxin (Figure 5D), which does not necessarily mean that they are hypersensitive. An increased signal was expected because both mutants already had increased activity without the addition of auxin, indicating that *trn* mutants are able to respond to auxin. The initial auxin transport into the young leaf primordia and basipetal generation of the midvein (Avsian-Kretchmer et al., 2002; Aloni et al., 2003; Mattsson et al., 2003) all occur in *trn* mutants, although the position of the distal focus and, thus, also the midvein is often shifted toward one side of the leaf. In hypocotyls, polar auxin transport is not reduced, and antibodies against different PIN proteins, putative facilitators of auxin efflux, are correctly localized in 5-d-old primary roots of both *trn* mutants (data not shown).

These data argue for normal auxin transport in very young seedlings and primordia and make it unlikely that the auxin transport machinery itself is affected directly. However, the ectopic PDR5:GUS activity at the leaf margins is clearly linked with the malformation of secondary and higher-order veins. Auxin is produced ectopically along the margins and may not be correctly sensed or transported toward the midvein, with incomplete vasculature as a consequence. Such deficiencies in auxin response or distribution could also explain the ectopic PDR5:GUS activity seen in adult leaves. High PDR5:GUS activity is observed in the wild type along leaf margins when grown on 10 μM 1-*N*-naphthylphthalamic acid and coincides with the abnormal formation of concentrated venation at the margins (Mattsson et al., 1999). No such concentration of veins along the margins is observed in *trn* mutants, arguing against auxin transport being the limiting factor for the formation of higher-order veins. We propose that both *TRN* genes are necessary for the canalization of the auxin signal into the formation of procambium, either by sensing/responding to auxin signals or by regulation of the auxin transport machinery. The prolonged and ectopic expression of *PCYCB1-1*:*GUS* along the vasculature in *trn1-1* suggests local alterations in cell division during vascular development, which could explain the formation of thicker veins, as is apparent in *trn*

mutants. Thus, the *TRN* genes are important for vascular meristem identity by participating in setting up the correct balance between cell proliferation and differentiation, which is necessary to maintain the continuity of vessels and sieve tubes.

Overall organ growth along the different growth axes and the initiation of vascular tissue occur in *trn* mutants simultaneously with those of the wild type. However, the anatomical data, cell size measurements, PCYCB1-1:GUS activity, and flow cytometry profile indicate that on the cellular level, cells in leaf primordia are not in the same phase of development as in the wild type. Cells in *trn* organs might possibly be impaired in their ability to respond to hormonal and/or additional developmental cues that are required for the coordinated formation of procambial higher-order veins. Previously, we have demonstrated the importance of *TRN1* and *TRN2*/*TET1* in the patterning of the primary root epidermis (Cnops et al., 2000). Root epidermal patterning results from signaling processes that lead to tissue specification along the radial axis. Mutants defective in either *TRN1* or *TRN2*/*TET1* affect cell fates of both root hair and non–root hair cells. Perhaps TRN2 and TRN1 act in the same pathway that recognizes a signaling molecule derived from the underlying cortical cell (or the intercellular space between two cortical cells), resulting in the determination of epidermal cell fate. In addition to incorrect epidermal patterning, both *trn* mutants also have altered lateral root cap identity and root growth defects. Based on their similar roles in patterning and growth in both roots and leaves, the phenotype conferred by *trn1 trn2*, and their protein structure, we postulate that TRN1 and TRN2/TET1 act in the same signaling process to coordinate patterning and growth at early leaf and root development.

METHODS

TRN1 Gene Cloning

Websites used for the analysis were as follows: Smart (http://smart.embl-heidelberg.de), Structural Classification of Proteins (http://scop.mrc-lmb.cam.ac.uk/scop/), BLAST (http://www.ncbi.nlm.nih.gov/BLAST), The Institute for Genomic Research (TIGR; http://tigrblast.tigr.org/tgi/), TMHMM (http://www.cbs.dtu.dk/services/TMHMM/), targetP, (http://www.cbs.dtu.dk/services/TargetP/), and Pfam (http://www.sanger.ac.uk/cgi-bin/Pfam). *trn1-4* was isolated from mutagenized *Arabidopsis thaliana* seed populations transformed with the activation-tagging vector pSK105 (Weigel et al., 2000). After cosegregation of a single T-DNA insertion with *trn1* phenotypes had been confirmed, the insertion site was determined by plasmid rescue, followed by sequencing reactions performed with T-DNA–specific primers. The T-DNA insert was found at position 3826 bp of the *TRN1* coding sequence. Homologous genes in other plant species were determined with the TIGR database and include sorghum (*Sorghum bicolor*; accession number TC20671), *Medicago truncatula* (TC1111561), rice (*Oryza sativa*; AAR87265), pine (*Pinus taeda*; DR119311), cotton (*Gossypium hirsutum*; CO082135), maize (*Zea mays*; CO449207), and soybean (*Glycine max*; CO980870).

Sequence Analysis of *TRN2* Homologs

MatDB was scanned for TRN2 homologs with BLAST. A hidden Markov model–based profile was created for these proteins with the HMMER package (Eddy, 1998) and was used to rescan the in-house database of predicted proteins in *Arabidopsis*, built with the EuGène program (Schiex et al., 2001; http://www.inra.fr/bia/T/EuGene). Automatic annotation of the selected proteins was improved. First, intron–exon borders were verified and the transcripts were aligned to the genomic region with Sim4 (Florea et al., 1998). Second, prediction errors were detected by aligning the proteins with each other. All of this information was compiled with ARTEMIS (Mural, 2000) and used to decide on the final gene structure.

Phylogenetic Analysis

The GenBank nonredundant protein database and the TIGR gene indices database (http://www.tigr.org/tdb/tgi) were scanned with BLAST for sequences homologous with *TRN2*, and the results were inspected manually. Sequences were aligned with ClustalW version 1.84, followed by manual alignment. Trees were constructed on conserved positions of the alignment by clustered EST sequences that contained a full open reading frame, full-length cDNA sequences (when available), and predicted rice and *Arabidopsis* genes with the neighbor-joining algorithm as implemented in TREECON (Van de Peer and De Wachter, 1994) and by Bayesian tree inference with MrBayes (Ronquist and Huelsenbeck, 2003) using the GTR+γ evolutionary model with six Markov chains for 500,000 generations, of which the first 50,000 were discarded. Alignments were edited and reformatted with ForCon (Raes and Van de Peer, 1999) and BioEdit (Hall, 1999). The statistical significance of nodes in the neighbor-joining approach was tested with 500 bootstrap replicates.

Expression Analysis and in Situ Hybridization

Total RNA was isolated from 50 to 100 mg of tissue and isolated with the RNeasy plant mini kit (Qiagen). cDNA was obtained by reverse transcription of 3 to 5 μg of RNA with SuperScript II reverse transcriptase according to the manufacturer's instructions (Invitrogen).

Probes were generated by PCR with primers carrying the T7 and T3 RNA polymerase binding sites at the 5′ end (TRN1-T7, 5′-CCAAGCTTCTAATACGACTCACTATAGGGAGAAGAGAACTACGGGAGACGACTGA-3′; TRN1-T3, 5′-AATTAACCCTCACTAAAGGGAGAAGCTGCTCTTTGTTCTTGTTC-3′; TRN2-T7, 5′-CCAAGCTTCTAATACGACTCACTATAGGGAGAAACTACCATTTGCCCTGA-3′; and TRN2-T3, 5′-AATTAACCCTCACTAAAGGGAGAAGCACCCGATAATGTAGACGATAA-3′). Labeling with digoxigenin (DIG) was performed with DIG RNA labeling mix (Roche Diagnostics) with either T3 or T7 RNA polymerase (Roche Diagnostics) according to the manual. Labeled probes were dissolved in 100 μL of water.

Seedlings (7 d old) were fixed in PBS + 4% paraformaldehyde overnight at 4°C. Material was dehydrated in ethanol and subsequent HistoClear (National Diagnostics) series. Embedding was performed at 60°C by adding paraffin and changing the solution eight times. Embedded material was cut with a RM2245 microtome (Leica) in 8-μm-thick sections that were transferred on charged slides. Paraffin was removed in HistoClear and ethanol series followed by 0.2 M HCl treatment for 20 min. Proteins were digested by treating sections for 20 min with 5 μg/mL proteinase K at 37°C, and the tissue was stabilized by fixation with 4% paraformaldehyde in PBS. Hybridization, washing, and antibody incubation were performed in an InsituPro VS robot (Intavis). Slides were treated twice with prehybridization buffer (20% formamide and 2.5% 20× SSC [1× SSC is 0.15 M NaCl and 0.015 M sodium citrate] in water). Samples were hybridized with antisense and sense probes (15 μL/mL) for 8 h at 50°C in hybridization buffer (40% formamide, 25% 20× SSC, 1% 100×Denhardt's solution [1× Denhardt's solution is 0.02% Ficoll, 0.02% polyvinylpyrrolidone, and 0.02% BSA], 1% yeast t-RNA [10 mg/mL], and 100 mg/mL salmon sperm DNA in water). Each washing step was performed three times: 3× SSC, 1.5× SSC, 0.75× SSC, and 0.3× SSC. Subsequent steps were done at room temperature. Samples were washed in Tris-buffered saline (TBS) with 0.2% Triton X-100 (TBST) and blocked with TBST + 3% BSA for 1 h. Incubation with anti-DIG-UTP-alkaline

phosphatase FAB fragments (1:2000; Roche Diagnostics) was done for 2 h. After washing with TBS, samples were equilibrated in detection buffer (100 mM Tris-HCl, pH 9.5, 100 mM NaCl, and 50 mM $MgCl_2$) and stained overnight with nitroblue tetrazolium chloride and 5-bromo-4-chloro-3-indolyl phosphate (Carl Roth) at 0.2 mM final concentration. Slides were mounted in 50% glycerol and inspected with an inverted microscope (Zeiss). Images were taken with a digital camera (Zeiss) and processed with AxioVision LE software (Zeiss).

Plant Material and Growth Conditions

The *trn2-1* mutation was in Col-4, *trn1-1* in C24, *trn1-2* in Ws ecotype (see Table 1 in Cnops et al., 2000), and *trn1-4* in a mixed Col-0 and Nossen background; *as1-1* (N3374) was in Col-1 and *PATHB8*:*GUS* (N296) was in Ws; they were obtained from the Nottingham Arabidopsis Seed Stock Centre. The *PDR5:GUS* and *PCYCB1-1*:*GUS* lines were kindly provided by B. Scheres (Department of Molecular Cell Biology, Utrecht University) and L. De Veylder (Ghent University), respectively. Plants were grown as described by Cnops et al. (2004).

Leaf Morphology and Histology

Cotyledons and fully expanded leaves of 4-week-old seedlings grown in vitro were cleared with 100% methanol (overnight) and subsequently with 90% lactic acid (overnight), photographed, and analyzed with the computer program Scion Image Beta 3b (Scion Corporation). Epidermal cell area was measured with differential interference contrast optics on cleared leaves.

To compare mutant and wild-type measurements, data were introduced into the Statistical Package for the Social Sciences (release 10.0.5; SPSS) (Cnops et al., 2004). Historesin-embedded leaf blades of fully expanded leaves were sectioned serially and stained with toluidine blue. The palisade cell number was determined as described (Nelissen et al., 2003). For visualization of callose in phloem sieve elements, 20-d-old seedlings were fixed and stained with 0.005% aniline blue (Carland et al., 1999).

Two-week-old *trn1-1*, *trn2-1*, C24, and Col-4 seedlings containing the *PDR5*:*GUS* marker were incubated in 90% acetone at 4°C for 30 min, washed in 50 mM sodium phosphate buffer with 0.01% Triton X-100, preincubated in phosphate buffer, pH 7, with 2 mM potassium ferricyanide/ferrocyanide for 30 min at 39°C, and subsequently incubated in 2 mM K_3/K_4 FeCN and 3 mM X-Gluc in phosphate buffer at 37°C for 4 h after 15 min of vacuum infiltration. The seedlings were washed and cleared overnight in 100% methanol. For *PATHB8*:*GUS*, 5- to 8-d-old seedlings of *trn2-1* and Col were incubated in X-Gluc for 2 h, and *trn* plant material containing *PCYCB1-1*:*GUS* was incubated for 1 h. *trn2-1* and Col-4 first or second leaves containing the *PDR5*:*GUS* marker gene were dissected from 13- and 16-d-old seedlings stained with GUS and fixed overnight at 4°C in 2.5% (v/v) glutaraldehyde in 50 mM sodium phosphate buffer. The leaves were dehydrated stepwise and embedded in Technovit (Heraeus). The fixed specimens were mounted by stitching a plastic support to the fixed blocks overnight with Technovit 3040. Sections (5 μm) were visualized under a dark field. For auxin response analysis, first leaves of 10-d-old seedlings were excised, incubated for 7 h in liquid germination medium, and histochemically analyzed.

Flow Cytometry

The *trn* mutants (*trn1-2* and *trn2-4*) were heterozygotes, allowing the leaves of *trn* and wild-type segregants from the same plate to be harvested. For each time point, two biological and three technical repeats were performed. The procedure was according to De Veylder et al. (2001).

Auxin Transport

Transport assays consisted of at least two individual experimental sets of 30 to 50 replicates each. To obtain elongated hypocotyls, 19-d-old plants were grown in darkness for 24 h. This treatment was performed for 100 h before hypocotyl excision. Sections of hypocotyl (5 mm) or stem (5 to 10 mm) were incubated upside-up or upside-down in a 500-μL Eppendorf tube containing 40 μL of growth medium solidified with 0.5% agar and 280 μCi of [^{3}H]IAA (3-[5(n)-^{3}H]indolyl acetic acid; 26 Ci/mmol [GE Healthcare]) and unlabeled IAA (400 pmol; Sigma-Aldrich) to obtain a final IAA concentration of 2×10^{-5} M. The explant was vertically submerged into the agar over a length of 2 to 3 mm, incubated for 18 h, removed from the substrate, and cut into two equal parts: an upper part never in contact with the substrate, and a lower part continuously incubated. The two parts were extracted for 24 h in 100 μL of 100% methanol, a 1000-μL scintillation cocktail was added (Ultima Gold; Packard), and the samples were assayed for tritium with a liquid scintillation counter (Tri-Carb 1500; Canberra Packard International). Total radioactivity was calculated as the sum of the radioactivity present in the upper (free) and lower (substrate) sites of the segment after incubation. Data are expressed as percentages of the total radioactivity present in the upper (free) site of the hypocotyl (stem). Acropetal (basipetal) transport of IAA corresponded to nonspecific (specific) transport from the basal to the apical (apical to basal) end of the segment obtained by assaying the explants in the upside-up (upside-down) position. As an additional control, 10^{-5} M 1-*N*-naphthylphthalamic acid (a kind gift from W. Michalke, University of Freiburg) was added in both positions to block polar auxin transport.

Auxin Analysis

Samples were ground in liquid nitrogen and extracted overnight in 80% methanol at −20°C. As a standard for isotope dilution purposes, 138 pmol of [$^{13}C_6$]IAA ([phenyl-$^{13}C_6$]indole-3-acetic acid) (Cambridge Isotope Laboratories) was added. IAA was purified by a combined solid-phase extraction, methylated, and analyzed by micro liquid chromatography-electrospray (+)-tandem mass spectrometry (Prinsen et al., 1998).

Accession Numbers

The Nottingham Arabidopsis Stock Centre codes for the *trn1-1* and *trn2-1* alleles are N9550 and N9551, respectively. The accession numbers of the genes are At5g55540 (*TRN1*) and At5g46700 (*TRN2*).

Supplemental Data

The following materials are available in the online version of this article.

Supplemental Figure 1. Map-Based Cloning of *TRN2*.

Supplemental Figure 2. Alignment of the *Arabidopsis* TET Proteins, Functional Domains, and *trn* Alleles.

Supplemental Figure 3. Sequence Alignment Used for the Phylogenetic Tree of Plant Tetraspanins in NEXUS Format.

Supplemental Figure 4. PDR5:GUS Activity in a Transverse Section of a *trn* Leaf.

ACKNOWLEDGMENTS

The authors thank Karen Cornelis, Jan Zethof, Janny Peters, Tom Gerats, and Andrea Falcone for help with *TRN2* and *TRN1* gene cloning; Sevgi Oden for hormone measurements; Xugang Li for antibody production; Wolfgang Michalke for providing 1-*N*-naphthylphthalamic acid; Gerrit Beemster, Tom Beeckman, and Kristiina Himanen for critical discussions; and Dirk Inzé and Harry Van Onckelen for support. This

work was supported by grants from the Interuniversity Poles of Attraction Program–Belgian Science Policy (P4/15 and P5/13), the Austrian Science Fund, the European Community's Human Potential Program under contract HPRN-CT-2002-00267 (DAGOLIGN), the Deutsche Forschungsgemeinschaft (SFB 592), the Fond der Chemischen Industrie, and the Bundesministerium für Bildung und Forschung. M.P. and H.N. are indebted to the European Union for a training grant in the frame of the project PREDEC (HPMT-CT-2000-00088) and the Institute for the Promotion of Innovation by Science and Technology in Flanders for a postdoctoral fellowship, respectively.

Received December 19, 2005; revised January 27, 2006; accepted February 16, 2006; published March 10, 2006.

REFERENCES

Aloni, R., Schwalm, K., Langhans, M., and Ullrich, C.I. (2003). Gradual shifts in sites of free-auxin production during leaf-primordium development and their role in vascular differentiation and leaf morphogenesis in *Arabidopsis.* Planta **216,** 841–853.

Avsian-Kretchmer, O., Cheng, J.-C., Chen, L., Moctezuma, E., and Sung, Z.R. (2002). Indole acetic acid distribution coincides with vascular differentiation pattern during Arabidopsis leaf ontogeny. Plant Physiol. **130,** 199–209.

Baima, S., Nobili, F., Sessa, G., Lucchetti, S., Ruberti, I., and Morelli, G. (1995). The expression of the *Athb-8* homeobox gene is restricted to provascular cells in *Arabidopsis thaliana.* Development **121,** 4171–4182.

Beemster, G.T.S., De Veylder, L., Vercruysse, S., West, G., Rombaut, D., Van Hummelen, P., Galichet, A., Gruissem, W., Inzé, D., and Vuylsteke, M. (2005). Genome-wide analysis of gene expression profiles associated with cell cycle transitions in growing organs of Arabidopsis. Plant Physiol. **138,** 734–743.

Belkhadir, Y., Subramaniam, R., and Dangl, J.L. (2004). Plant disease resistance protein signaling: NBS-LRR proteins and their partners. Curr. Opin. Plant Biol. **7,** 391–399.

Byrne, M.E., Barley, R., Curtis, M., Arroyo, J.M., Dunham, M., Hudson, A., and Martienssen, R.A. (2000). *Asymmetric leaves1* mediates leaf patterning and stem cell function in *Arabidopsis.* Nature **408,** 967–971.

Candela, H., Martínez-Laborda, A., and Micol, J.L. (1999). Venation pattern formation in *Arabidopsis thaliana* vegetative leaves. Dev. Biol. **205,** 205–216.

Carland, F.M., Berg, B.L., FitzGerald, J.N., Jinamornphongs, S., Nelson, T., and Keith, B. (1999). Genetic regulation of vascular tissue patterning in Arabidopsis. Plant Cell **11,** 2123–2137.

Carland, F.M., and McHale, N.A. (1996). *LOP1*: A gene involved in auxin transport and vascular patterning in *Arabidopsis.* Development **122,** 1811–1819.

Cnops, G., den Boer, B., Gerats, T., Van Montagu, M., and Van Lijsebettens, M. (1996). Chromosome landing at the Arabidopsis *TORNADO1* locus using an AFLP-based strategy. Mol. Gen. Genet. **253,** 32–41.

Cnops, G., Jover-Gil, S., Peters, J.L., Neyt, P., De Block, S., Robles, P., Ponce, M.R., Gerats, T., Micol, J.L., and Van Lijsebettens, M. (2004). The *rotunda2* mutants identify a role for the *LEUNIG* gene in vegetative leaf morphogenesis. J. Exp. Bot. **55,** 1529–1539.

Cnops, G., Wang, X., Linstead, P., Van Montagu, M., Van Lijsebettens, M., and Dolan, L. (2000). *TORNADO1* and *TORNADO2* are required for the specification of radial and circumferential pattern in the *Arabidopsis* root. Development **127,** 3385–3394.

De Veylder, L., Beeckman, T., Beemster, G.T.S., Krols, L., Terras, F., Landrieu, I., Van Der Schueren, E., Maes, S., Naudts, M., and Inzé, D. (2001). Functional analysis of cyclin-dependent kinase inhibitors of Arabidopsis. Plant Cell **13,** 1653–1667.

Diévart, A., and Clark, S.E. (2004). LRR-containing receptors regulating plant development and defense. Development **131,** 251–261.

Donnelly, P.M., Bonetta, D., Tsukaya, H., Dengler, R.E., and Dengler, N.G. (1999). Cell cycling and cell enlargement in developing leaves of *Arabidopsis.* Dev. Biol. **215,** 407–419.

Eddy, S.R. (1998). Profile hidden Markov models. Bioinformatics **14,** 755–763.

Florea, L., Hartzell, G., Zhang, Z., Rubin, G.M., and Miller, W. (1998). A computer program for aligning a cDNA sequence with a genomic DNA sequence. Genome Res. **8,** 967–974.

Hall, T.A. (1999). BioEdit: A user-friendly biological sequence alignment editor and analysis program for Windows 95/98/NT. Nucleic Acids Symp. Ser. **41,** 95–98.

Hemler, M.E. (2001). Specific tetraspanin functions. J. Cell Biol. **155,** 1103–1107.

Hemler, M.E. (2003). Tetraspanin proteins mediate cellular penetration, invasion, and fusion events and define a novel type of membrane microdomain. Annu. Rev. Cell Dev. Biol. **19,** 397–422.

Huang, S., et al. (2005). The phylogenetic analysis of tetraspanins projects the evolution of cell–cell interactions from unicellular to multicellular organisms. Genomics **86,** 674–684.

Inohara, N., Chamaillard, M., McDonald, C., and Nuñez, G. (2005). NOD-LRR proteins: Role in host-microbial interactions and inflammatory disease. Annu. Rev. Biochem. **74,** 355–383.

Iwakawa, H., Ueno, Y., Semiarti, E., Onouchi, H., Kojima, S., Tsukaya, H., Hasebe, M., Soma, T., Ikezaki, M., Machida, C., and Machida, Y. (2002). The *ASYMMETRIC LEAVES2* gene of *Arabidopsis thaliana*, required for formation of a symmetric flat leaf lamina, encodes a member of a novel family of proteins characterized by cysteine repeats and a leucine zipper. Plant Cell Physiol. **43,** 467–478.

Kang, J., and Dengler, N. (2002). Cell cycling frequency and expression of the homeobox gene *ATHB-8* during leaf vein development in *Arabidopsis.* Planta **216,** 212–219.

Koizumi, K., Naramoto, S., Sawa, S., Yahara, N., Ueda, T., Nakano, A., Sugiyama, M., and Fukuda, H. (2005). VAN3 ARF-GAP-mediated vesicle transport is involved in leaf vascular network formation. Development **132,** 1699–1711.

Ljung, K., Bhalerao, R.P., and Sandberg, G. (2001). Sites and homeostatic control of auxin biosynthesis in *Arabidopsis* during vegetative growth. Plant J. **28,** 465–474.

Maecker, H.T., Todd, S.C., and Levy, S. (1997). The tetraspanin superfamily: Molecular facilitators. FASEB J. **11,** 428–442.

Mattsson, J., Ckurshumova, W., and Berleth, T. (2003). Auxin signaling in Arabidopsis leaf vascular development. Plant Physiol. **131,** 1327–1339.

Mattsson, J., Sung, Z.R., and Berleth, T. (1999). Responses of plant vascular systems to auxin transport inhibition. Development **126,** 2979–2991.

Mural, R.J. (2000). *ARTEMIS*: A tool for displaying and annotating DNA sequence. Brief. Bioinform. **1,** 199–200.

Nadeau, J.A., and Sack, F.D. (2003). Stomatal development: Cross talk puts mouths in place. Trends Plant Sci. **8,** 294–299.

Nelissen, H., Clarke, J.H., De Block, M., De Block, S., Vanderhaeghen, R., Zielinski, R.E., Dyer, T., Lust, S., Inzé, D., and Van Lijsebettens, M. (2003). DRL1, a homolog of the yeast TOT4/KTI12 protein, has a function in meristem activity and organ growth in plants. Plant Cell **15,** 639–654.

Olmos, E., Reiss, B., and Dekker, K. (2003). The *ekeko* mutant demonstrates a role for tetraspanin-like protein in plant development. Biochem. Biophys. Res. Commun. **310,** 1054–1061.

Peters, J.L., Cnops, G., Neyt, P., Zethof, J., Cornelis, K., Van Lijsebettens, M., and Gerats, T. (2004). An AFLP-based genome-wide mapping strategy. Theor. Appl. Genet. **108,** 321–327.

Pien, S., Wyrzykowska, J., McQueen-Mason, S., Smart, C., and Fleming, A. (2001). Local expression of expansin induces the entire process of leaf development and modifies leaf shape. Proc. Natl. Acad. Sci. USA **98,** 11812–11817.

Prinsen, E., Van Dongen, W., Esmans, E.L., and Van Onckelen, H.A. (1998). Micro and capillary liquid chromatography tandem mass spectrometry: A new dimension in phytohormone research. J. Chromatogr. A **826,** 25–37.

Raes, J., and Van de Peer, Y. (1999). ForCon: A software tool for the conversion of sequence alignments. EMBnet.news **6,** http://www.ebi.ac.uk/embnet.news/vol6_1.

Ronquist, F., and Huelsenbeck, J.P. (2003). MrBayes 3: Bayesian phylogenetic inference under mixed models. Bioinformatics **19,** 1572–1574.

Schiex, T., Moisan, A., and Rouzé, P. (2001). EUGÈNE: An eukaryotic gene finder that combines several sources of evidence. Lect. Notes Comput. Sci. **2066,** 111–125.

Semiarti, E., Ueno, Y., Tsukaya, H., Iwakawa, H., Machida, C., and Machida, Y. (2001). The *ASYMMETRIC LEAVES2* gene of *Arabidopsis thaliana* regulates formation of a symmetric lamina, establishment of venation and repression of meristem related homeobox genes in leaves. Development **128,** 1771–1783.

Stipp, C.S., Kolesnikova, T.V., and Hemler, M.E. (2003). Functional domains in tetraspanin proteins. Trends Biochem. Sci. **28,** 106–112. Erratum. Trends Biochem. Sci. **28,** 124.

Sun, Y., Zhou, Q., Zhang, W., Fu, Y., and Huang, H. (2002). *ASYMMETRIC LEAVES1*, an *Arabidopsis* gene that is involved in the control of cell differentiation in leaves. Planta **214,** 694–702.

Turner, S., and Sieburth, L.E. (2002). Vascular patterning. In The Arabidopsis Book, C.R. Somerville and E.M. Meyerowitz, eds (Rockville, MD: American Society of Plant Biologists), doi/10.1199/tab.0073, http://www.aspb.org/publications/arabidopsis/.

Van de Peer, Y., and De Wachter, R. (1994). TREECON for Windows: A software package for the construction and drawing of evolutionary trees for the Microsoft Windows environment. Comput. Appl. Biosci. **10,** 569–570.

Verkest, A., de O. Manes, C.-L., Vercruysse, S., Maes, S., Van Der Schueren, E., Beeckman, T., Genschik, P., Kuiper, M., Inzé, D., and De Veylder, L. (2005). The cyclin-dependent kinase inhibitor KRP2 controls the onset of the endoreduplication cycle during Arabidopsis leaf development through inhibition of mitotic CDKA;1 kinase complexes. Plant Cell **17,** 1723–1736.

Weigel, D., et al. (2000). Activation tagging in Arabidopsis. Plant Physiol. **122,** 1003–1013.

Wyrzykowska, J., Pien, S., Shen, W.H., and Fleming, A.J. (2002). Manipulation of leaf shape by modulation of cell division. Development **129,** 957–964.

Zgurski, J.M., Sharma, R., Bolokoski, D.A., and Schultz, E.A. (2005). Asymmetric auxin response precedes asymmetric growth and differentiation of *asymmetric leaf1* and *asymmetric leaf2* Arabidopsis leaves. Plant Cell **17,** 77–91.